Hindawi
Mathematical Problems in Engineering
Volume 2022, Article ID 3524734, 18 pages
https://doi.org/10.1155/2022/3524734

Research Article

An Accurate Mathematical Model and Experimental Research of Pressure Distribution in the Spool Valve Clearance Film

Jia Chen, Fei Li, and Yi Yang

School of Electronic Engineering, Xi'an Shiyou University, No. 18, East Section of Electronic 2nd Road, Xi'an, Shannxi, China

Correspondence should be addressed to Fei Li; lif@xsyu.edu.cn

Received 17 April 2022; Accepted 10 September 2022; Published 22 November 2022

Academic Editor: Hao Zhang

As an actuator control element of the electrohydraulic system in aerospace, airplanes, and other equipment, the spool valve is prone to the "hydraulic lock" problem, which may cause major accidents of these electrohydraulic systems. The grooves engraved on the spool can effectively eliminate this problem by migrating the uneven pressure distribution in the clearance film between the sleeve and the spool. The effect of migrating uneven pressure distribution depends on the groove parameters. This paper proposed an accurate mathematical model with rectangular grooves to investigate the effect. Unlike previous mathematical models based on the Reynolds equation, the proposed model is based on the Navier–Stokes equation, which is more valid in the range where the clearance film thickness is much less than the groove depth. Meanwhile, the mathematical model takes the distributions, width, depth, and the number of grooves into consideration. Then, the proposed mathematical model was used to investigate the effects of mitigating the uneven pressure distribution under various parameters of grooves. To verify the accuracy of the mathematical model, the volume flow leakage in the clearance film obtained by the proposed model and the Reynolds equation, respectively, is compared with that obtained by the experimental test. The comparison results indicate that the results obtained by the Reynolds equation could reach a maximum of 14.75% different from the experimental results, while the results obtained by the NS equation are only 5.57% different under the same conditions, implying that the mathematical model derived from the NS equation is more accurate.

1. Introduction

As the amplifier stage of an electrohydraulic system, the spool valve provides control over the direction and flow of the fluid, which is widely used in various hydraulic actuators that can be utilized to control the aircraft rudder surface deflexion, control the drilling steering, control the turning of a ship, and so on. Therefore, the spool valve affects the hydraulic actuator's position control accuracy, speed control accuracy, and force control accuracy. However, the spool-type valves are susceptible to a unique problem known as hydraulic lock due to the uneven pressure distribution in the clearance film between the spool and the sleeve. The uneven pressure distribution around the spool creates a lateral force which causes the spool to tilt at a small angle. Then, the lateral force increases with the tiny angle and makes the tilted angle greater so that the spool contacts with the inner wall of the sleeve, resulting in the spool locking in the sleeve. The spool locking phenomena cause the actuator of hydraulic equipment to fail and even cause safety accidents, as shown in Figure 1. In theory, the locking problem could be avoided when the clearance exactly parallels with the sleeve's walls. However, in practice, the perfectly parallel walls between spools and sleeves are not obtainable due to the limitations of tooling machines. Fortunately, some circumferential grooves applied on the spool surfaces can be used to decrease the lateral force to limit the effects of locking phenomena.

The first study about limiting the hydraulic locking phenomena was conducted by Sweeney [1], who presented that some grooves along the spool axial direction can mitigate uneven pressure distributions in the clearance film. Since then, several researchers [2–10] have utilized the Reynolds equation to investigate the lubricant characteristics

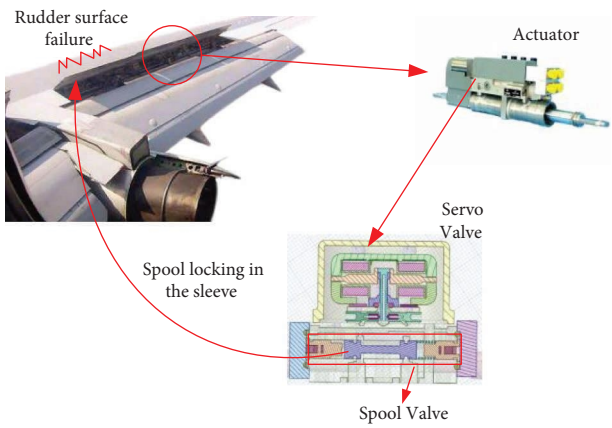

Figure 1: Rudder surface of airplane failure caused by spool locking in the sleeve.

of the clearance film of the spool valve. For instance, the pressure in each groove and the leakage in the clearance film were calculated by Milani [10] based on the Reynolds equation. Since the Reynolds equation is derived from the NS equation, Dong et al. [11] compared the difference of pressure distribution between the Reynolds equation and the NS equation and found that the difference exceeds 20% when the clearance film is greater than 0.413 μm. Furthermore, Guardino et al. [12] investigated the difference in various values of the roughness amplitude to the clearance film ratio and pointed out that the difference increases with the ratio. In the following years, some research results [13–18] used in hydrostatic gas-lubricated tribological components obtained the same results as those in reference [12]. Simultaneously, the research methods based on the NS equation are applicable to the study of the clearance film lubrication between the sleeve and the spool as the depth of the groove to the thickness of the clearance film ratio is greater than ten [19, 20]. Therefore, Hong and Kim [20] used computational fluid dynamics (CFD) based on the NS equation to compare spiral grooves' migrating uneven pressure distribution effects and traditional grooves. The uneven pressure distribution was simulated for different inlet pressure conditions [21]. It was found that the uneven pressure increased linearly with the inlet pressure. Unfortunately, the study [21] did not investigate the effect of grooves on eliminating uneven pressure. Meanwhile, CFD was widely utilized to study the effect of different types of grooves on improving load-carrying capacity and film stiffness in gas face seals [22–25]. Load-carrying capacity and film stiffness in the gas face seal are related to the type of grooves and the geometric values of grooves. However, load-carrying capacity and leakage rate are conflicted. In other words, the improvement of load-carrying capacity increases the leakage rate, which must be as small as possible for the gas face seal. Aiming to take into account load-carrying capacity and volume flow leakage, Wang et al. [26] firstly established an accurate mathematical model of grooves and then utilized this mathematical model to optimize the groove shapes using the multiobjective optimization approach, which is very mature in the present time. Thus, the accurate mathematical model of grooves is the most important for the multiobjective optimization of groove shapes. Unfortunately, the current mathematical models of the clearance film pressure distribution between the sleeve and the spool are based on the Reynolds equation. The difference of pressure distribution in the spool valve between the Reynolds equation and the NS equation increases with width, depth, and number of grooves [27].

Therefore, an accurate mathematical model of clearance film pressure distribution in the spool valve is established based on the NS equation in cylindrical coordinates in this paper. Meanwhile, this accurate mathematical model takes into account the distribution, width, depth, and the number of grooves and is used to investigate the lateral force and the volume flow leakage under various groove geometric dimensions. To verify the mathematical model, an experiment is tested to compare with the theoretical results obtained by the NS equation and the Reynolds equation, respectively.

2. Description of the Spool Valve Structure

The spool valves are utilized to amplify the hydraulic energy in the servo valve, as shown in Figure 2(a), and to control the flow's direction and flow in the spool valve system, as shown in Figure 2(b). Figure 2(c) illustrates that the spool valve consists of the sleeve and the spool, and a spool usually has several lands. For the convenience of calculation, the mathematical model of one land is first established. Thus, the geometry of the spool can be simplified as Figure 2(d). The simplified spool with radius r_{sp} and length $2l$ is nested in the sleeve with the radius r_{sl}. The spool is stationary with a tilted angle α in the sleeve.

The classical groove applied to the spool mostly forms a circular groove with a rectangular cross-sectional area. The parameters of the groove consist of the distance between the groove and the spool edge, the distance l_3 between grooves, the width l_2 of groove, and the depth h_z of the groove, as shown in Figure 2(d). Supposing that the number of the grooves is n, the length of the spool can be written as

$$2l_1 + nl_2 + (n-1)l_3 = 2l. \tag{1}$$

The geometric dimensions of the spool and the groove are tabulated in Table 1. The length of spool l, the radius of the spool r_{sp}, the inner radius of the sleeve r_{sl}, and l_1 are all constant, which do not affect the lubricant characteristics of the clearance film between the spool and the sleeve. Besides, the aspect ratio K represents the groove depth h_z to the groove width l_2 ratio, the width of the spool l_2, the distance between grooves l_3, and the tilted angle α which are variable geometric dimensions of the spool, which need to investigate the effect on the lubricant characteristics.

3. Mathematical Model

As shown in Figure 2(d), taking into account the cylindrical shape of the spool and the sleeve, the NS equations in cylindrical coordinates are written as

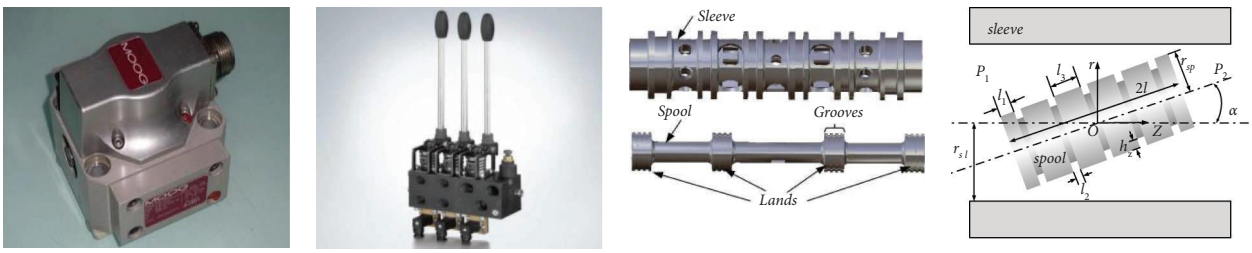

(a) (b) (c) (d)

Figure 2: Schematic of the spool valve with rectangular grooves: (a) servo valve, (b) spool valve group, (c) spool valve, and (d) schematic of the spool valve.

Table 1: Geometrics of the spool valve.

Parameters	Value
l (mm)	7.98
l_1 (mm)	1.5
l_2 (mm)	1.0, 0.8, 0.6, 0.4, 0.2
l_3 (mm)	0.1, 0.2, 0.4, 0.8, 1.6
K	0.125, 0.25, 0.5, 1
r_{sl} (mm)	6
r_{sp}(mm)	5.99
α (degree)	0.0288, 0.0188
n (number of grooves)	2, 4, 6, 8

$$\begin{cases} \rho\left(\dfrac{\mathrm{Dv}_r}{\mathrm{Dt}} - \dfrac{v_\theta^2}{r}\right) = \rho f_r - \dfrac{\partial P}{\partial r} + \mu\left(\nabla^2 v_r - \dfrac{v_r}{r^2} - \dfrac{2}{r^2}\dfrac{\partial v_\theta}{\partial \theta}\right), \\ \rho\left(\dfrac{\mathrm{Dv}_\theta}{\mathrm{Dt}} + \dfrac{v_r v_\theta}{r}\right) = \rho f_\theta - \dfrac{1}{r}\dfrac{\partial P}{\partial \theta} + \mu\left(\nabla^2 v_r - \dfrac{v_\theta}{r^2} + \dfrac{2}{r^2}\dfrac{\partial v_r}{\partial \theta}\right), \\ \rho\dfrac{\mathrm{Dv}_z}{\mathrm{Dt}} = \rho f_z - \dfrac{\partial P}{\partial z} + \mu\nabla^2 v_z, \end{cases} \tag{2}$$

where

$$\begin{cases} \dfrac{D}{\mathrm{Dt}} = \dfrac{\partial}{\partial t} + v_r\dfrac{\partial}{\partial r} + \dfrac{v_\theta}{r}\dfrac{\partial}{\partial \theta} + v_z\dfrac{\partial}{\partial z}, \\ \nabla^2 = \dfrac{\partial^2}{\partial r^2} + \dfrac{1}{r}\dfrac{\partial}{\partial r} + \dfrac{1}{r^2}\dfrac{\partial^2}{\partial \theta^2} + \dfrac{\partial^2}{\partial z^2}. \end{cases} \tag{3}$$

The sleeve and the spool are both assumed to be stationary. In addition, the tilted angle of the spool is small enough that the flow in the clearance film between the spool and sleeve moves approximately along the z-direction. The terms for velocity in the NS equation thereby can be written as

$$\begin{cases} v_\theta = v_r \approx 0,\ v_z = v_z(r,\theta), \\ \dfrac{\partial P}{\partial \theta} = 0,\ \dfrac{\partial P}{\partial r} = 0,\ \dfrac{\partial P}{\partial z} = \dfrac{\mathrm{dp}}{\mathrm{dz}}. \end{cases} \tag{4}$$

When (4) is substituted into (2), and the second-order differential terms in (2) are reduced, (2) can be written as

$$\frac{d^2 v_z}{\mathrm{dr}^2} + \frac{1}{r}\frac{\mathrm{dv}_z}{\mathrm{dr}} = \frac{1}{\mu}\frac{\mathrm{dP}}{\mathrm{dz}}. \tag{5}$$

The integral general solution of fluid velocity v_z can be listed as follows:

$$v_z = \frac{r^2}{2}C_1 \ln r + C_2 + \frac{r^2 \ln r}{2\mu}\frac{\mathrm{dP}}{\mathrm{dz}} - \frac{r^2}{4\mu}\frac{\mathrm{dP}}{\mathrm{dz}}(2\ln r - 1), \tag{6}$$

where μ is the fluid's dynamic viscosity, r is the radius with O as the center, and C_1 and C_2 are both constants.

According to the assumption above, v_z equals zero when r in (6) equals the radius r_{sl}. When r equals r_z which is the distance from the center O to the wall of the spool, r_z equals zero since the spool is stationary. r_z is a variable parameter, the value of which is related to the center distance $\overline{\mathrm{OO}}_{\mathrm{sp}}$ and the rotary angle θ, that needs to be calculated using the longitudinal section illustrated in Figure 3. Due to the very small tilted angle α, the longitudinal section of the spool is approximately circular whose center is O_{sp}, and the radius is $r_{\mathrm{sp}}' = r_{\mathrm{sp}}\cos\alpha$. As shown in Figure 3, the eccentricity direction is assumed to coincide with the angles increasing in the clockwise direction. Then, the analytical expression for r_z can be deduced as follows:

$$r_z = r_{\mathrm{sp}}' - \overline{\mathrm{OO}}_{\mathrm{sp}}\cos\theta - h_z. \tag{7}$$

Introducing the boundary conditions and putting (7) into (6) by linearizing $\ln r$ to ζr, the fluid velocity v_z in the clearance film becomes

$$v_z = \frac{1}{4\mu}\frac{\mathrm{dP}}{\mathrm{dz}}\left(r^2 - r(r + r_z) - r_{\mathrm{sl}} r_z\right), \tag{8}$$

where the term ζr is eliminated in the calculation, and thus, the effect on the calculation of linearization above is ignored.

The differential element of volume flow leakage in the clearance film can be written as

$$\mathrm{dQ} = 2\pi \mathrm{r} \mathrm{v}_z \mathrm{dr}, \tag{9}$$

where the range of r is from r_z to r_{sl}. Integrating (9), Q can be expressed as

$$\mathrm{Q} = 2\pi\int_{r_z}^{r_{\mathrm{sl}}} v_z r \mathrm{dr}. \tag{10}$$

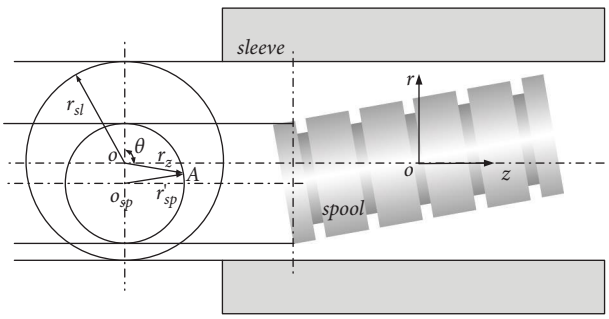

Figure 3: The longitudinal section of the spool.

Introducing (8) into (10), the integration for Q is solved as follows:

$$Q = \frac{2\pi r_z}{8\mu}\frac{\mathrm{dP}}{\mathrm{dz}}\left(r_{sl} + r_z\right)^2. \tag{11}$$

According to (11), the analytical expression of the pressure gradient along the z-axis becomes

$$\frac{\mathrm{dP}}{\mathrm{dz}} = \frac{8\mu Q}{2\pi r_z\left(r_z + r_{\mathrm{sl}}\right)^2}. \tag{12}$$

Since the range of spools in the z-axis is from $-l$ to l, the pressure distribution in the clearance film can be written in (13) by solving a definite integral pressure gradient:

$$P = \frac{-8\mu Q}{2\pi r_{\mathrm{sl}}\tan\alpha\cos\theta} f(z) + C_3, \tag{13}$$

where C_3 is a constant, and $f(z)$ is a function with z as its argument. According to an integral part of (12), $f(z)$ is expressed as

$$f(z) = \ln\left|z - \frac{r'_{\mathrm{sp}} - h_z}{\tan\alpha\cos\theta}\right| + \ln\left|z - \frac{r'_{\mathrm{sp}} - h_z + r_{sl}}{\tan\alpha\cos\theta}\right| - \frac{r_{\mathrm{sl}}}{z\tan\alpha\cos\theta - r'_{\mathrm{sp}} - h_z - r_{\mathrm{sl}}}. \tag{14}$$

For the pressure distribution at both ends of the spool, the first boundary conditions are $P = P_2$ and $z = l$, and the second boundary conditions are $P = P_1$ and $z = -l$. Thus, owing to the continuity of fluid, the constant C_3 can be written as

$$C_3 = P_2 + \left(P_2 - P_1\right)\frac{f(l)}{f(l) - f(-l)}. \tag{15}$$

The volume flow leakage in the clearance film is written as

$$Q = \frac{-\left(P_2 - P_1\right)r'_{\mathrm{sl}}\tan\alpha\cos\theta}{8\mu\left[f(l) - f(-l)\right]}. \tag{16}$$

Thus, from equation (13) to (15), we can obtain the following:

$$P = P_2 - \frac{8\mu Q}{r'_{\mathrm{sl}}\tan\alpha\cos\theta} f(z) + \left(P_2 - P_1\right)\frac{f(l)}{f(l) - f(-l)}. \tag{17}$$

The value of h_z in (14) is related to the z-axis coordinate value and the number of grooves. When the number is even, the value of h_z becomes

$$h_z = \left\{h_z \,\middle|\, z \in \pm\ \cos\alpha\left[\left|\left[\frac{l_3}{2} + (m-1)l_3 + (m-1)l_2, \frac{l_3}{2}\right\} + (m-1)l_3 + ml_2\right]\right\}, \tag{18}$$

where m is the number of grooves, and the value can be set as 1, 2, 3, . . ., $n/2$.

When the number is odd, the value of h_z becomes

$$h_z = \left\{h_z \,\middle|\, z \in \pm\ \cos\alpha\left[\frac{g(m)l_2}{2} + (m-1)l_3 + (m-2)l_2, \frac{l_2}{2} + (m-1)l_3 + (m-1)l_2\right]\right\}, \tag{19}$$

where the value of m can be set as 1, 2, 3, . . ., $(n+1)/2$, $g(m) = \begin{cases} 1, & m > 1, \\ 0, & m \le 1, \end{cases}$.

Equation (17) presents the pressure distribution in the clearance film between the spool and the sleeve, which can be used to calculate the lateral force by integrating the pressure P in the clearance film, as shown in (20). The decrease rate of the absolute value of the lateral force reflects the effect of eliminating the uneven pressure distribution around the spool [21]. The smaller the lateral force, the better the effect of eliminating the uneven pressure distribution:

$$F = \int_{-l}^{l}\int_{0}^{2\pi} \mathrm{P}\mathrm{d}r\mathrm{d}\theta. \tag{20}$$

4. Simulation Results

4.1. The Optimal Distribution of the Grooves. The optimal distribution of the grooves needs to be confirmed first. For the sake of investigating the effect of parameter l_3 on the pressure distribution in the clearance film, several cases are compared through calculating the pressure distribution and the lateral force based on the geometric dimensions tabulated in Table 1. Except for the parameter l_3, each case utilizes the same geometric dimensions, such as width ($l_2 = 0.8$ mm), depth ($K = 0.25$), and the number of grooves. Meanwhile, each case shares the same properties of the working fluid, as shown in Table 2, and utilizes different pressure conditions, as shown in Table 3. With the decrease of l_3, the grooves are clustered to the end edge of the spool ($l_3 = 0.1$ mm). When l_3 equals 1.6 mm, the grooves are evenly distributed.

Figure 4(b) illustrates that the lateral force has a minimum value in the case where the grooves are evenly distributed. And the equidistribution grooves have the same effect on the pressure distribution in the case of different pressure conditions and tilted angles, as shown in Figures 4(c) and 4(d).

Figures 4(c) and 4(d) also illustrate that the decreased slope of the lateral force with an increment of l_3 under a tilted angle, $\alpha = 0.0188^\circ$, is lower than that under the tilted angle $\alpha = 0.0288^\circ$. This is because the effect of grooves decreases with the reduction of tilted angle α. Nevertheless, compared with the lateral force at $l_3 = 0.1$ mm, the lateral force at $l_3 = 1.6$ mm is reduced by 16.9%, 14.9%, and 14.8% at pressure 5 MPa, 7 MPa, and 9 MPa, respectively. Same as the value of the lateral force, the uniformly distributed grooves provide a more effective lubricant characterized along the circumference, mitigating the unbalance pressure distribution. Figure 4(a) supports the effect, which is very approximate to the numerical results in reference [27]. Therefore, compared with other distributions of grooves, the even distribution groove is optimal.

4.2. The Effect of the Cross-Sectional of Groove on Lateral Force. Besides the distribution of grooves, the geometric dimensions also affect the value of the lateral force, such as the groove depth h_z and the groove width l_2 [27]. Therefore, it is essential to investigate the effect of these two parameters on the lateral force. As shown in Figures 5–7, the lateral force decreases with the increase in the width of the groove for the same value of K in cases where the number of grooves is 2, 4, 6, and 8, respectively. Meanwhile, the lateral force also decreases with the increment of the aspect ratio K for the same value of l_2. This is because the lateral force is related to the cross-sectional area which is proportional to the width l_2 and K, as shown in Figure 8. In other words, the increase in the value of the cross-sectional area indicates a decrease in the lateral force value. As a result, the increase in cross-sectional helps migrate the uneven pressure distribution surrounding the spool.

In addition, different increasing rates of cross-sectional area of the groove lead to different decreased slopes of the lateral force. For instance, as shown in Figure 5(a), the greater value of K leads to the greater increase rate of the cross-sectional area, which causes the greater decreased slope of the lateral force for the same increased rate of l_2. Similarly, different groove numbers result in different decreased slopes of the lateral force. As shown in Figure 9, for the same value of K and the same increased rate of the groove width l_2, the decreased slope of the lateral force increases with the increase in the groove number in the case where the pressure $P_1 = 7$ MPa and the tilted angle $\alpha = 0.288^\circ$. For example, in the case where $K = 0.25$, along with the same increased rate of l_2, the reduction rate of the lateral force is 3.35%, 5.91%, and 17.49% when the number of the grooves is eight compared with which is 1.73%, 2.89%, and 4.4% when the number of the groove is 4. This conclusion also applies to the reduction rates of the lateral force in cases of $P_1 = 5$ MPa and 9 MPa, respectively, and the tilted angle $\alpha = 0.188^\circ$, as tabulated in Tables 4–6.

Table 2: Properties of the working fluid.

Parameter of fluid	Value
Density ρ (kg/m^3)	839.3
$\mu(N \cdot s/m^2)$	0.0241

Table 3: Pressure condition.

Pressure	Value
P_1 (MPa)	5, 7, 9
P_2 (MPa)	0

According to the theoretical results above, the lateral force decreases with the increase in the groove number. However, the volume flow leakage increases with the increase in the groove number, which is illustrated in Figure 10. Meanwhile, the volume flow leakage increases with the increase of P_1 since the volume flow leakage is positively proportional to the differential pressure according to (16). As the sole driving energy of the spool, the differential pressure, as shown in (21), decreases when the volume flow leakage is too much. In other words, too much volume flow leakage causes the reduction of the driving force of the spool, to reduce the dynamic characteristic of the valve:

$$P_d = P_1 - P_2. \tag{21}$$

In addition, the strength of the spool reduces with the increase in groove depth. Therefore, the width of the groove, the depth of the groove, the number of the grooves, the leakage volume flow, and the strength of the spool need to be comprehensively considered when optimizing the parameters of the groove.

5. Experimental Verification

As for the second or third stage of the servo valve or other valves, the spool usually has more than one land. To conclude more closely to fit the actual situation, the second stage spool of the servo valve with four lands is investigated. Figure 11 shows the spool valve, and the spools with four lands are named as S_1, S_2, S_3, and S_4. As shown in Figure 11, P_1 and P_2 are the relatively high-pressure inlet and the

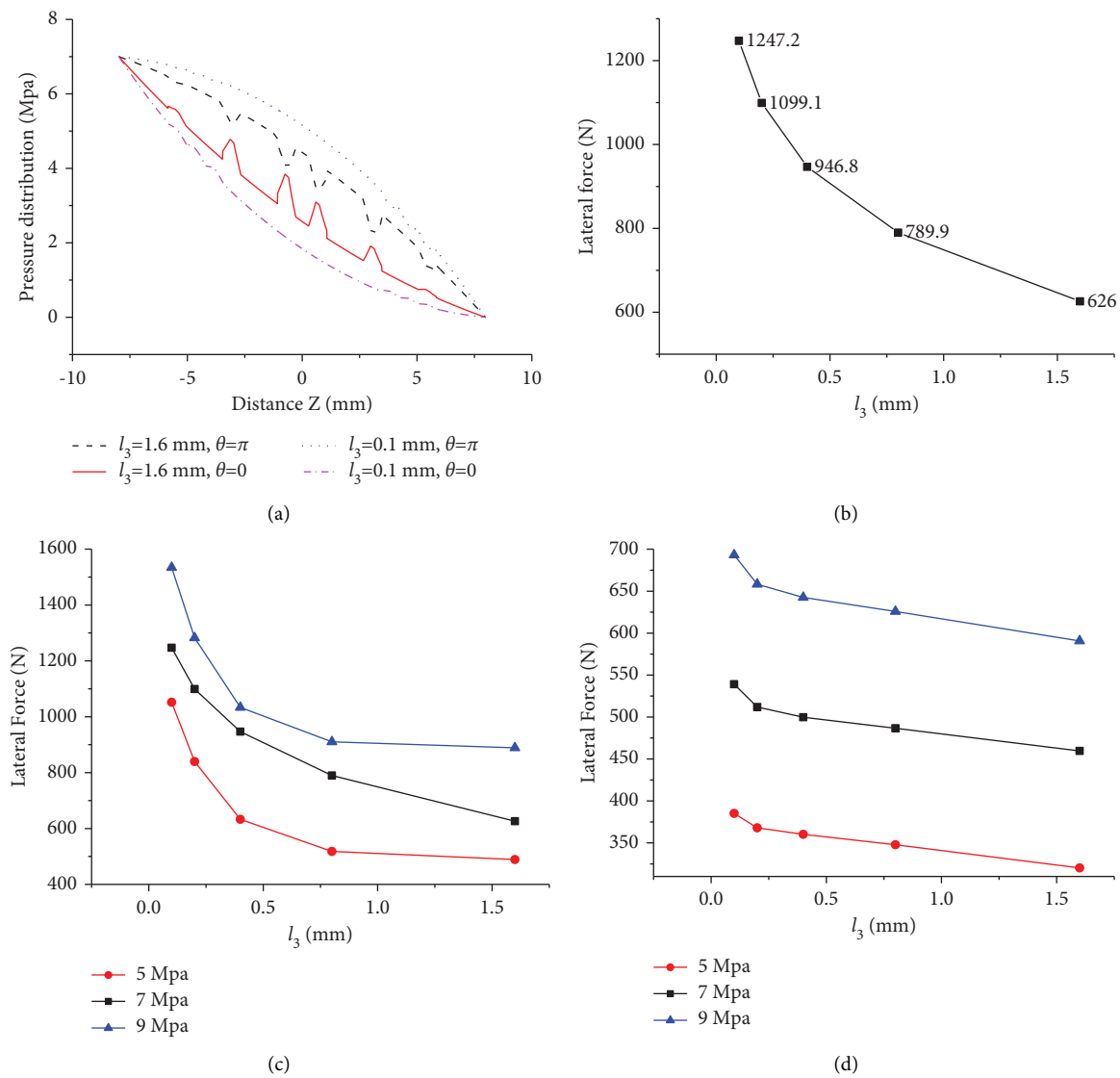

Figure 4: Lateral force and pressure distribution in cases of various values of the parameter l_3: (a) lateral force with l_3, (b) pressure distribution with distance Z, (c) tilted angle $\alpha = 0.0288^\circ$, and (d) tilted angle $\alpha = 0.0188^\circ$.

relatively low-pressure outlet, respectively, and P_A and P_B are the loading outlet of the servo valve.

The hydraulic diagram of the test bench is shown in Figure 12. The two overflow valves are used to change the supply oil pressure. The solenoid valve 4 is normally open. When the solenoid valves 1 and 2 are both turned on, and the solenoid valve 3 is turned off, the volume flow leakage between the land S_2 and the sleeve can be tested by flowmeter. Conversely, when the solenoid valves 1 and 3 are both turned on, and the solenoid valve 2 is turned off, the volume flow leakage between the land S_3 and the sleeve can be tested by flowmeter.

To verify the mathematical model derived above, the volume flow leakage rate between the spool and the sleeve is tested by the equipment setup illustrated in Figure 13. The test system consists of the oil supply system, the spool valve drive system, and the data acquisition system. In Figure 13(b), the spool valve drive system is composed of the stepper motor, and the spool valve is preinstalled and tilted at an angle α. The stepper motor propels the spool towards the positive direction of the z-axis until the port A is fully open. Meanwhile, port A is connected to the relatively high port, and port B is connected to the relatively low-pressure port. Then, the volume flow leakage between the land S_2 and the sleeve is measured by the flowmeter, that is shown in Figure 13(c). Conversely, when the spool was pulled in the negative direction of the z-axis, the volume flow leakage rate between the land S_3 and the sleeve was measured and recorded. Figure 13(d) presents the oil circuit connection photo at the bottom of the spool valve. Thus, S_2, S_3, and the sleeve can be obtained at different differential pressure values derived from the impairment between P_1 and P_2.

The oil supply system can provide different constant values of pressure, where the value of return oil is 0.3 MPa so that the value of P_2 is set as 0.3 MPa in the mathematical model. The boundary conditions of the land S_2 are shown in

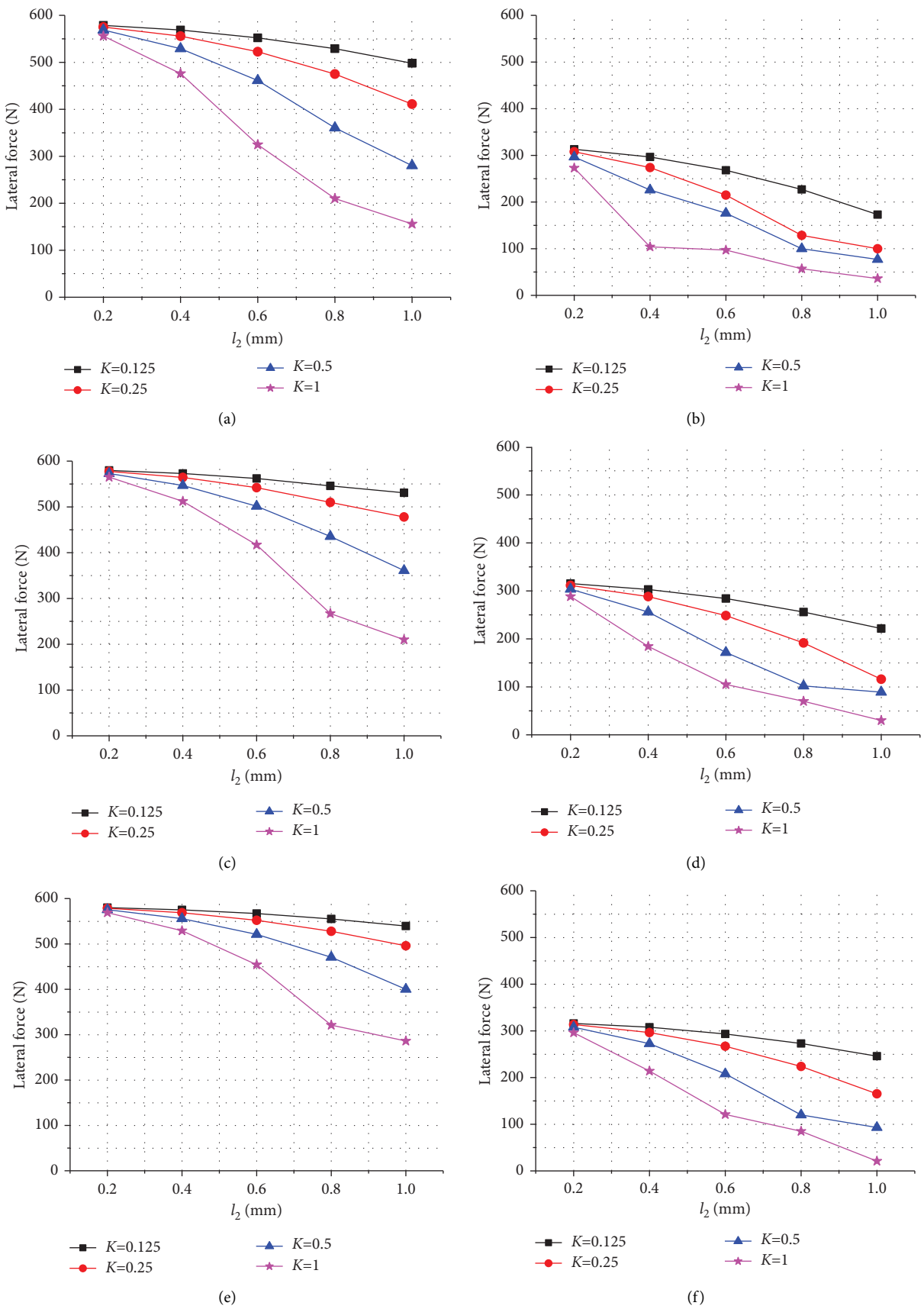

Figure 5: Continued.

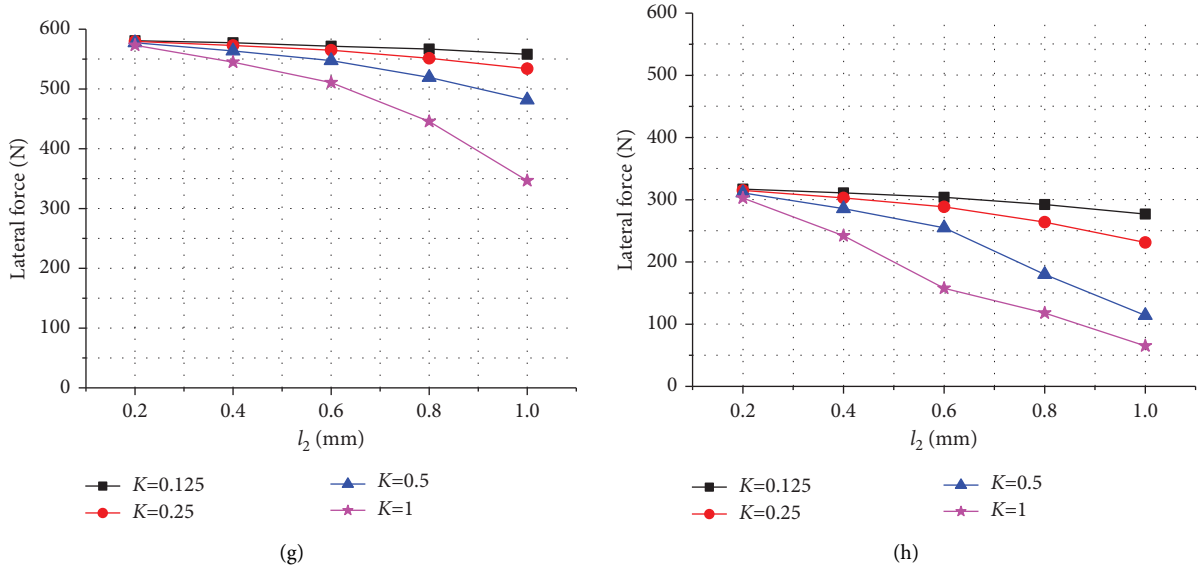

Figure 5: Lateral forces with variations of the value of K and the groove width in the case where $P_1 = 5$ MPa: (a) $n = 8$, $\alpha = 0.0288^\circ$, (b) $n = 8$, $\alpha = 0.0188^\circ$, (c) $n = 6$, $\alpha = 0.0288^\circ$, (d) $n = 6$, $\alpha = 0.0188^\circ$, (e) $n = 4$, $\alpha = 0.0288^\circ$, (f) $n = 4$, $\alpha = 0.0188^\circ$, (g) $n = 2$, $\alpha = 0.0288^\circ$, and (h) $n = 2$, $\alpha = 0.0188^\circ$.

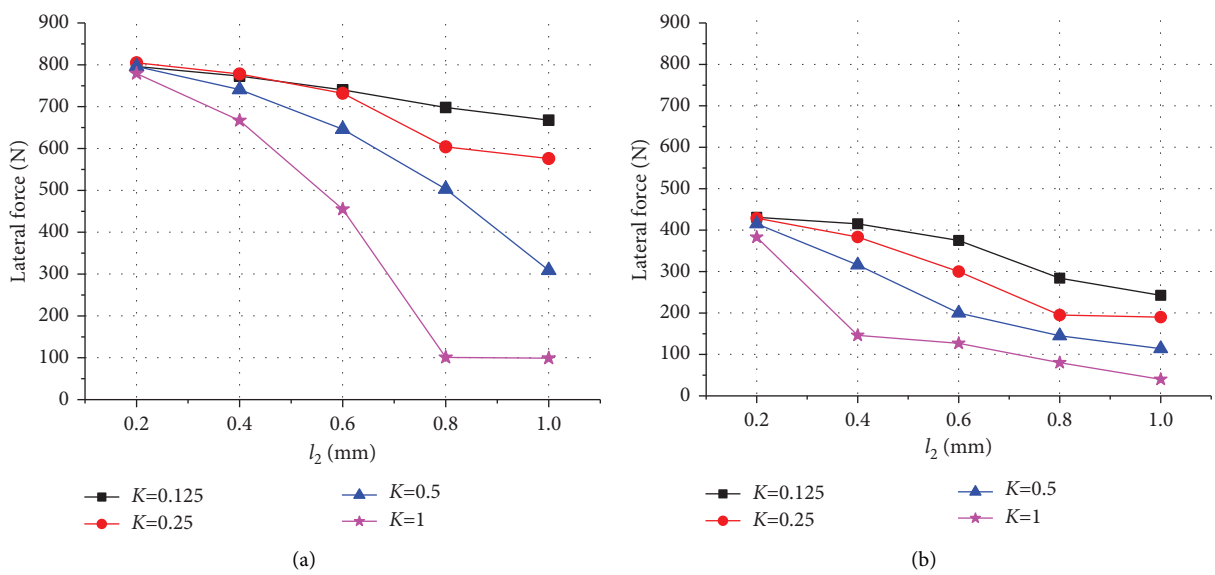

Figure 6: Continued.

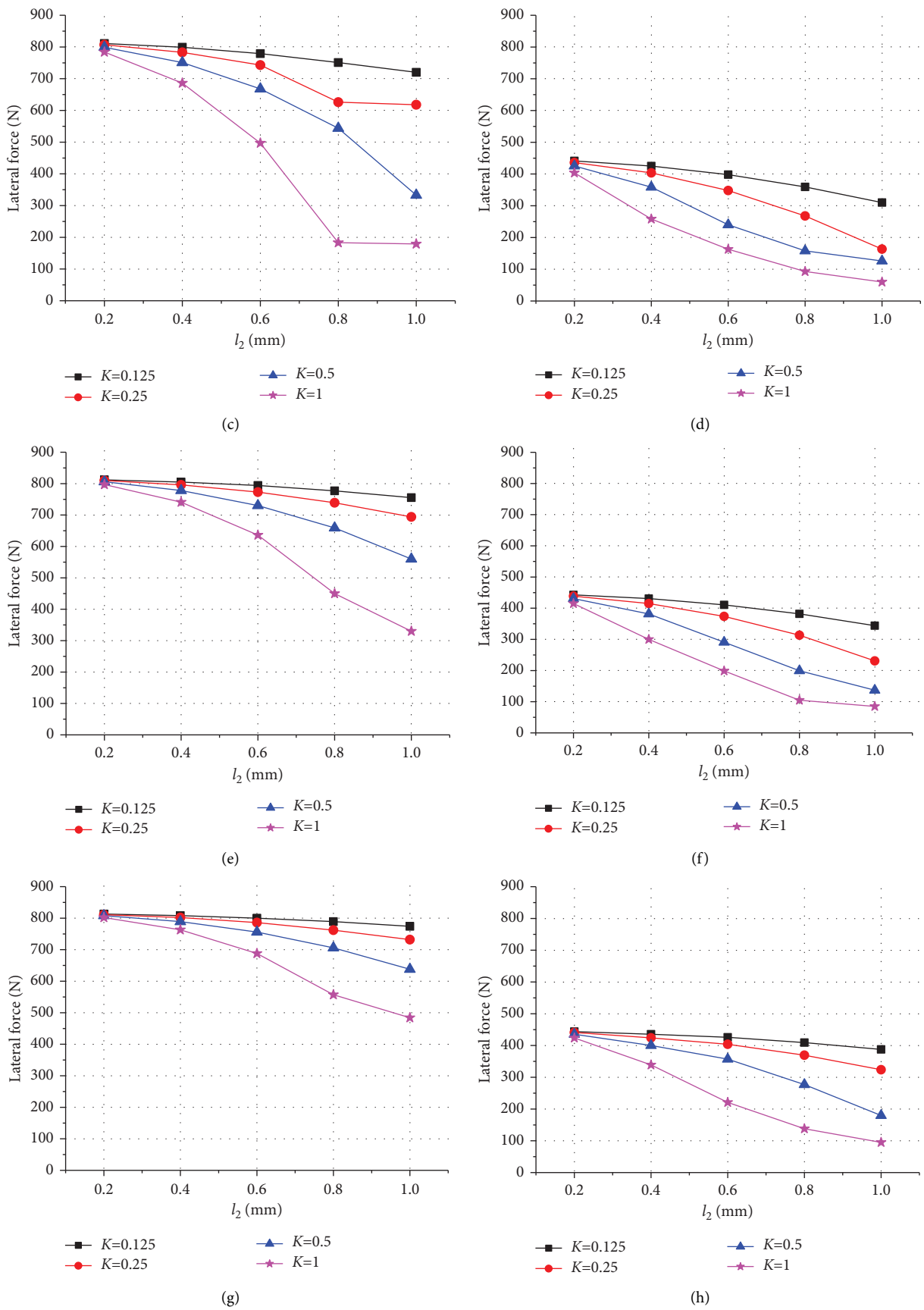

Figure 6: Lateral forces with variations of the value of K and the groove width in the case where $P_1 = 7$ MPa: (a) $n = 8$, $\alpha = 0.0288^\circ$, (b) $n = 8$, $\alpha = 0.0188^\circ$, (c) $n = 6$, $\alpha = 0.0288^\circ$, (d) $n = 6$, $\alpha = 0.0188^\circ$, (e) $n = 4$, $\alpha = 0.0288^\circ$, (f) $n = 4$, $\alpha = 0.0188^\circ$, (g) $n = 2$, $\alpha = 0.0288^\circ$, and (h) $n = 2$, $\alpha = 0.0188^\circ$.

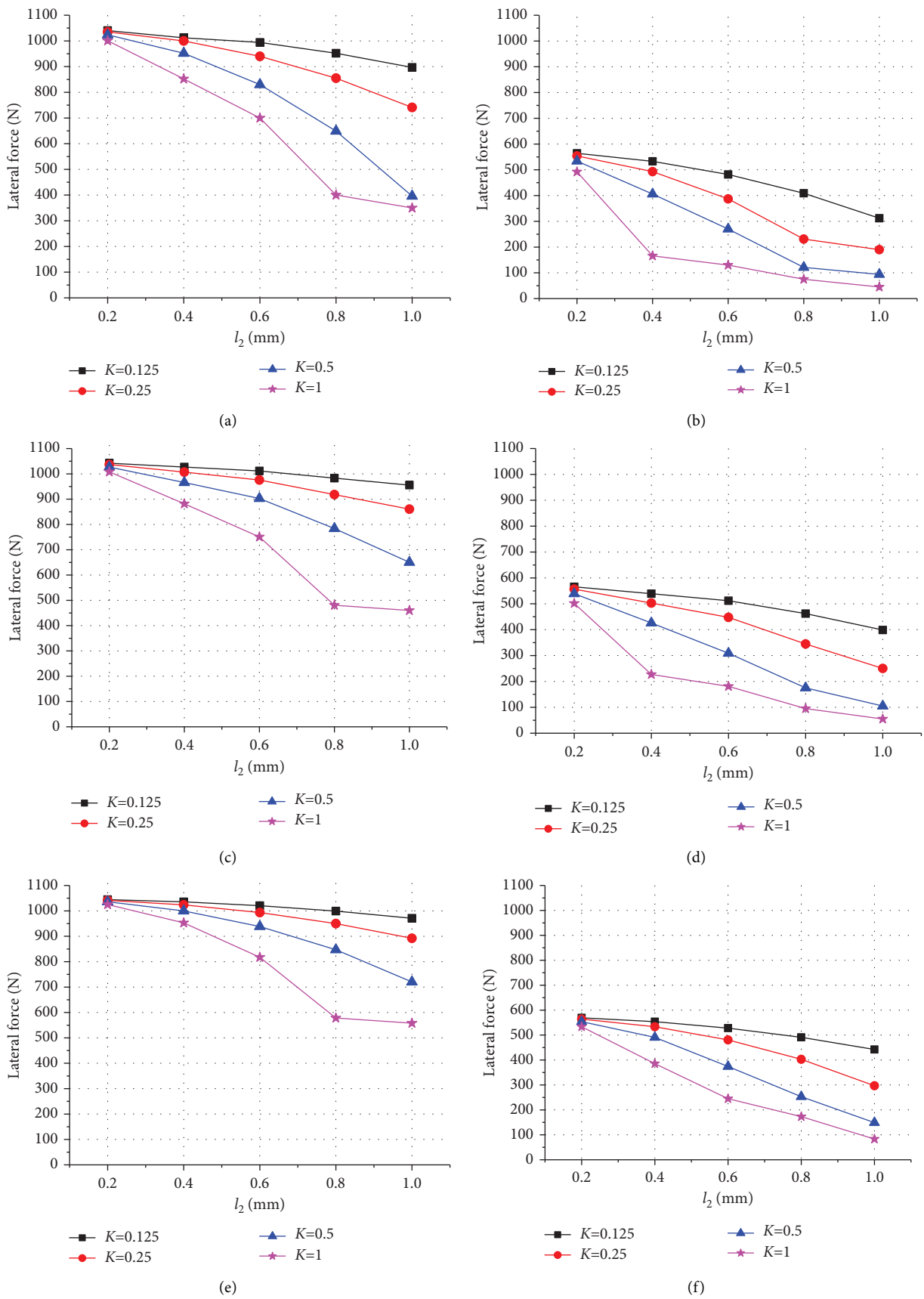

Figure 7: Continued.

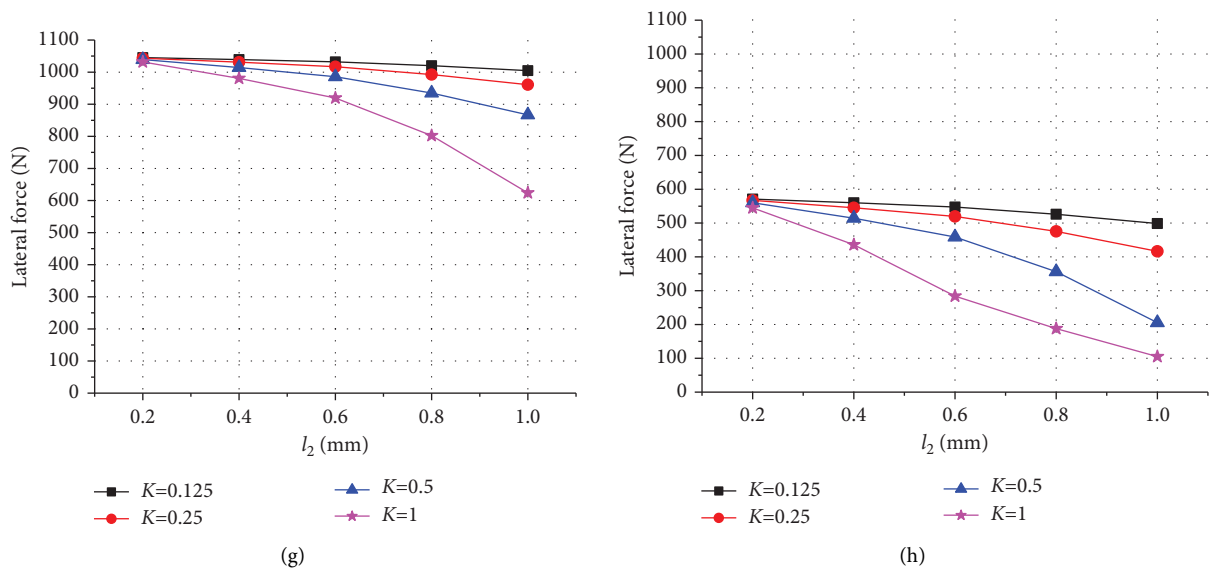

Figure 7: Lateral forces with variations of the value of K and the groove width in the case where $P_1 = 9$ MPa: (a) $n = 8$, $\alpha = 0.0288^\circ$, (b) $n = 8$, $\alpha = 0.0188^\circ$, (c) $n = 6$, $\alpha = 0.0288^\circ$, (d) $n = 6$, $\alpha = 0.0188^\circ$, (e) $n = 4$, $\alpha = 0.0288^\circ$, (f) $n = 4$, $\alpha = 0.0188^\circ$, (g) $n = 2$, $\alpha = 0.0288^\circ$, and (h) $n = 2$, $\alpha = 0.0188^\circ$.

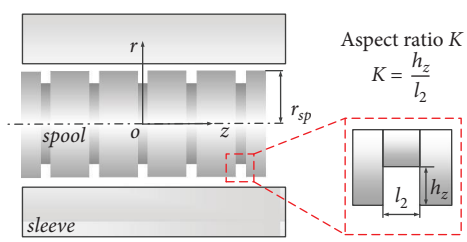

Figure 8: The cross-sectional area of the groove.

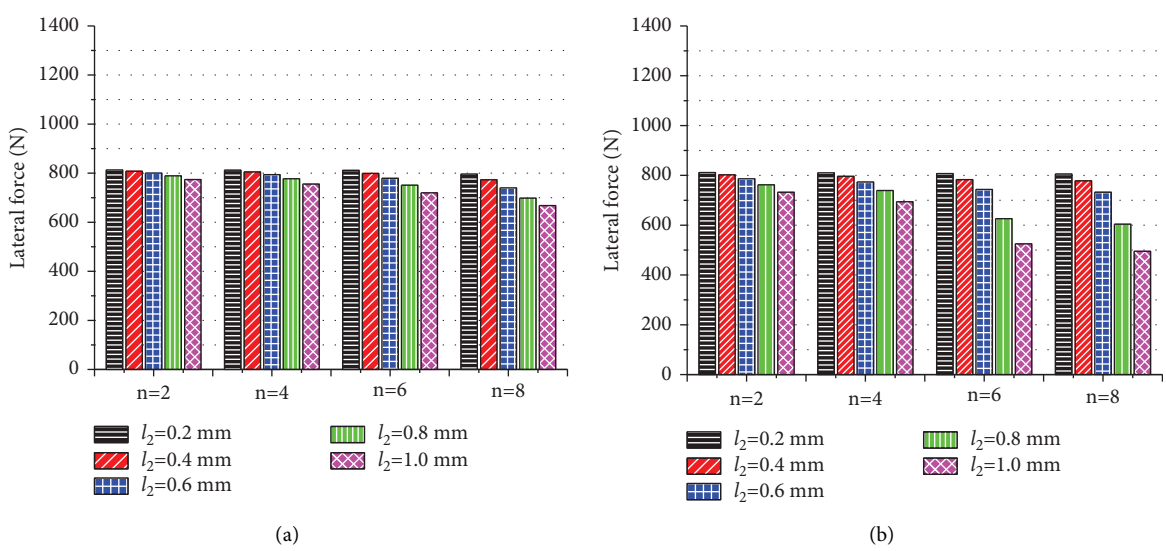

Figure 9: Continued.

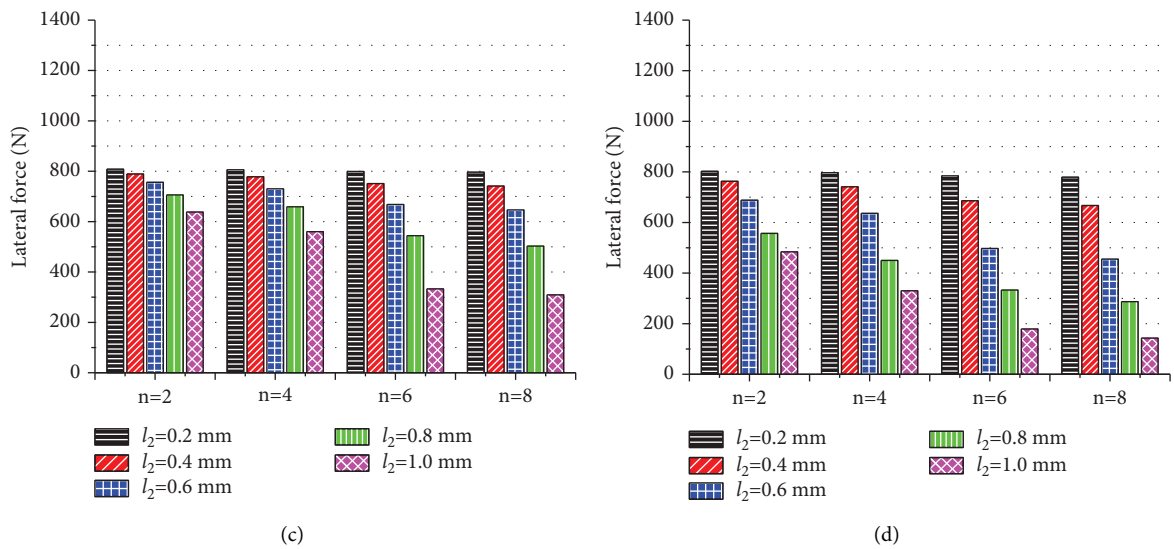

Figure 9: Lateral forces with variations of groove number and groove width in the case where $P_1 = 7$ MPa and $\alpha = 0.288^\circ$: (a) $K = 0.125$, (b) $K = 0.25$, (c) $K = 0.5$, and (d) $K = 1$.

Table 4: The percentage of lateral force reduction in the case where $P_1 = 5$ MPa.

	$n = 2$	$n = 4$	$n = 6$	$n = 8$
$K = 0.125$, $\alpha = 0.288$	0.5, 0.6, 0.8, 1.6	0.9, 1.4, 2.1, 2.8	1.2, 1.9, 2.8, 2.8	1.7, 2.9, 4.2, 5.9
$K = 0.25$, $\alpha = 0.288$	1.2, 1.4, 2.4, 3.2	1.7, 3.0, 4.4, 6.1	2.3, 4.0, 5.9, 6.3	3.4, 6.0, 9, 13.5
$K = 0.5$, $\alpha = 0.288$	2.4, 2.9, 5.1, 7.3	3.4, 6.7, 9.7, 17.7	4.6, 8.3, 13.2, 17	7.0, 12.8, 21.9, 22.3
$K = 1$, $\alpha = 0.288$	4.9, 6.3, 12.7, 22.2	7.0, 14.2, 29.3, 42	9.3, 18.6, 35.9, 43.8	14.4, 31.8, 35.3, 49
$K = 0.125$, $\alpha = 0.188$	1.9, 2.3, 3.9, 5.2	2.6, 4.7, 7.0, 9.9	3.9, 6.3, 9.9, 13.5	5.2, 9.6, 15.3, 23.8
$K = 0.25$, $\alpha = 0.188$	3.8, 4.8, 8.5, 12.4	5.5, 9.9, 16.2, 26.2	7.5, 13.7, 22.9, 75.5	11, 21.5, 40.1, 49.4
$K = 0.5$, $\alpha = 0.188$	8.2, 10.8, 29.4,36.6	11.5, 23.7, 32.3, 43.2	15.7, 32.9, 40.6, 42.1	23.9, 26.5, 39.7, 50
$K = 1$, $\alpha = 0.188$	19.9, 25, 35, 44.9	27.7, 29.7, 43.5, 75.3	36, 43, 57, 77.8	43.6, 47.4, 59.3, 78.8

Table 5: The percentage of lateral force reduction in the case where $P_1 = 7$ MPa.

	$n = 2$	$n = 4$	$n = 6$	$n = 8$
$K = 0.125$, $\alpha = 0.288$	0.6, 1.0, 1.4, 1.9	1.4, 2.1, 2.8, 7.6	1.5, 2.5, 3.6, 4.1	1.8, 2.9, 4.2, 4.3
$K = 0.25$, $\alpha = 0.288$	1.1, 2.0, 3.1.3.9	1.7, 2.9, 4.4, 6.1	3.0, 5.1, 15.7, 16.1	3.4, 5.9, 17.5, 18
$K = 0.5$, $\alpha = 0.288$	2.4, 4.2, 6.6, 9.6	3.5, 6.2, 9.7, 15	6, 11, 18.6, 38.8	6.9, 12,8, 22.1, 39
$K = 1$, $\alpha = 0.288$	4.9, 9.8, 13,19	7, 14.2, 29.2, 31.1	12.5, 27.6, 33, 46.2	14.4, 31.8, 36.9, 50.2
$K = 0.125$, $\alpha = 0.188$	1.9, 2.2, 3.9, 5.3	2.7, 4.7, 7, 9.9	3.6, 6.4, 9.7, 13.8, 14.5	5.2, 9.7, 16, 23
$K = 0.25$, $\alpha = 0.188$	3.9, 4.7, 8.5, 12.4	5.4, 9.9, 16.2, 26.3	7.5, 13,8, 23, 39	8, 21.7, 35, 42
$K = 0.5$, $\alpha = 0.188$	8.2, 10,8, 22.4, 35.1	11.4, 23.8, 31.5, 34.8	15.7, 33, 34.2, 38	23.9, 36.7, 40, 58.3
$K = 1$, $\alpha = 0.188$	20, 34.8, 37.5, 38.4	27.7, 33.7, 47.2, 52.3	36, 37, 42.9, 45.2	39.9, 44.8, 45.7, 50.7

Table 6: The percentage of lateral force reduction in the case where $P_1 = 9$ MPa.

	$n = 2$	$n = 4$	$n = 6$	$n = 8$
$K = 0.125$, $\alpha = 0.288$	0.6, 0.7, 1.2, 1.5	0.9, 1.4, 2.1,2.8	1.45, 1.5, 2.8, 2.8	2.7, 3, 3.1, 5.8
$K = 0.25$, $\alpha = 0.288$	1.2, 1.4, 2.4, 3.2	1.7, 3.0, 4.4, 6.1	2.9, 3.1, 5.9, 6.3	3.4, 6, 9, 13.3
$K = 0.5$, $\alpha = 0.288$	2.4, 2.8, 5.1, 7.3	3.5, 6.2, 9.7, 15	6.0, 6.5, 13.2, 17	7, 12.8, 21.8, 27
$K = 1$, $\alpha = 0.288$	4.9, 6.3, 12.7, 22.2	7, 14.2, 29.2, 31	12.5, 14.9, 36, 41	14.9, 17.8, 40, 43
$K = 0.125$, $\alpha = 0.188$	1.9, 2.3, 3.9, 5.2	2.7, 4.7, 7.0, 9.9	4.7, 5, 9.7, 13.7	5.5, 9.6, 15.1, 23.7
$K = 0.25$, $\alpha = 0.188$	3.8, 4.7, 8.5, 12.4	5.4, 9.9, 16.1, 26.3	9.7, 11, 23, 27.4	11, 21.5, 30, 42.6
$K = 0.5$, $\alpha = 0.188$	8.1, 10.8, 22.3, 42.4	11.4, 23.8, 32.4, 41.1	21, 27.5, 43.4, 44.9	23.9, 33.5, 45.1, 50
$K = 1$, $\alpha = 0.188$	20.1, 34.8, 33.9, 44	27.7, 36.5, 40, 45.6	29.9, 39, 45, 53.4	32.1, 43, 47.9, 54.5

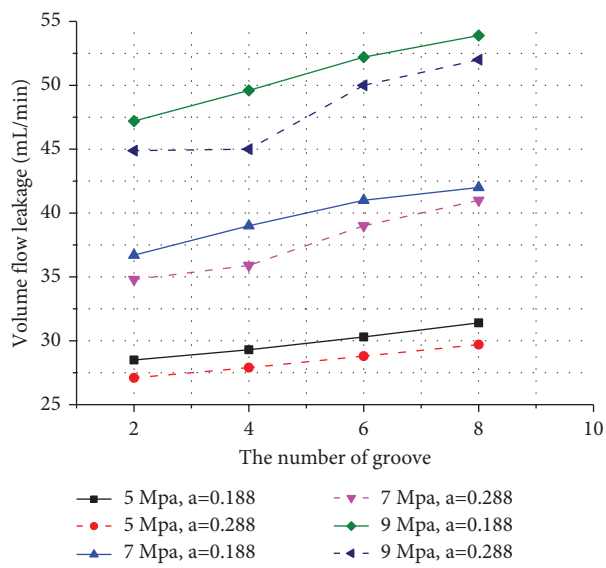

Figure 10: Volume flow leakage with different numbers of groove in case of different P_1.

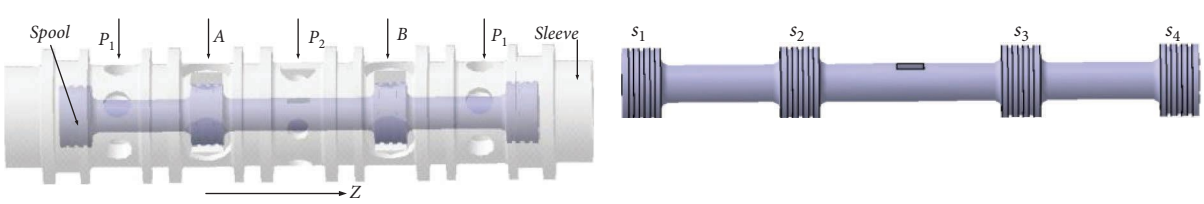

(a) (b)

Figure 11: Spool valve: (a) sleeve and (b) spool.

Figure 14. To keep the boundary conditions consistent with the theoretical calculation, the relatively high-pressure P_1 in the experiment is set as 5.3 MPa, 7.3 MPa, and 9.3 MPa, respectively, taking the spool valve used in hydraulic dives and control, where working pressure often reaches 35 MPa. The relatively high-pressure P_1 which equals 35.3 MPa is considered both in the simulation and experiment. Then, the differential pressure P_d in the experiment is the same as that in the theoretical calculation. Simultaneously, the number of the groove and the tilted angles of the spool are both taken the same values as the values of the theoretical calculation, as tabulated in Table 1.

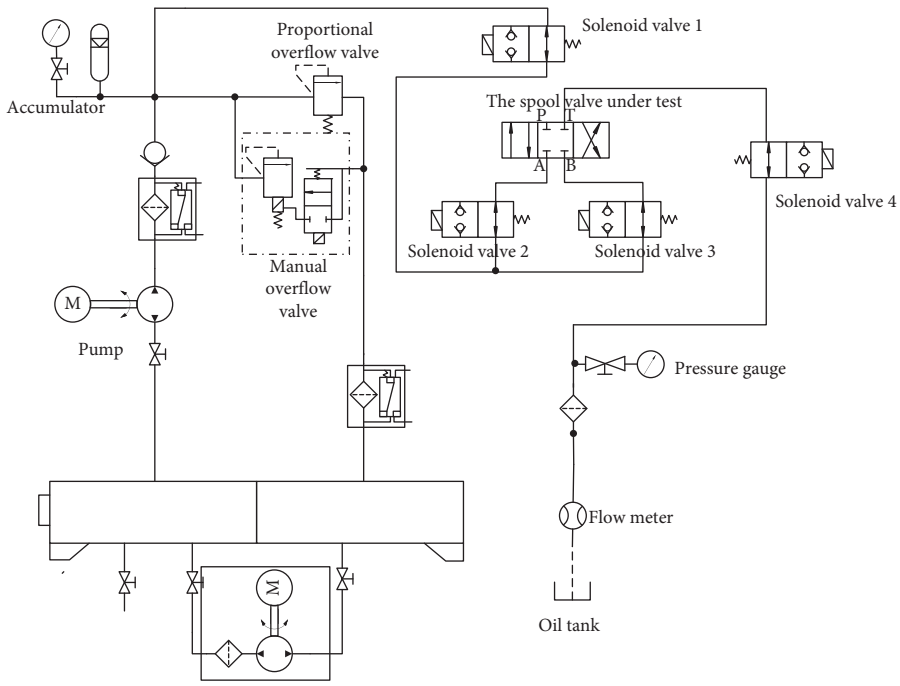

Figure 12: The hydraulic diagram of the test bench.

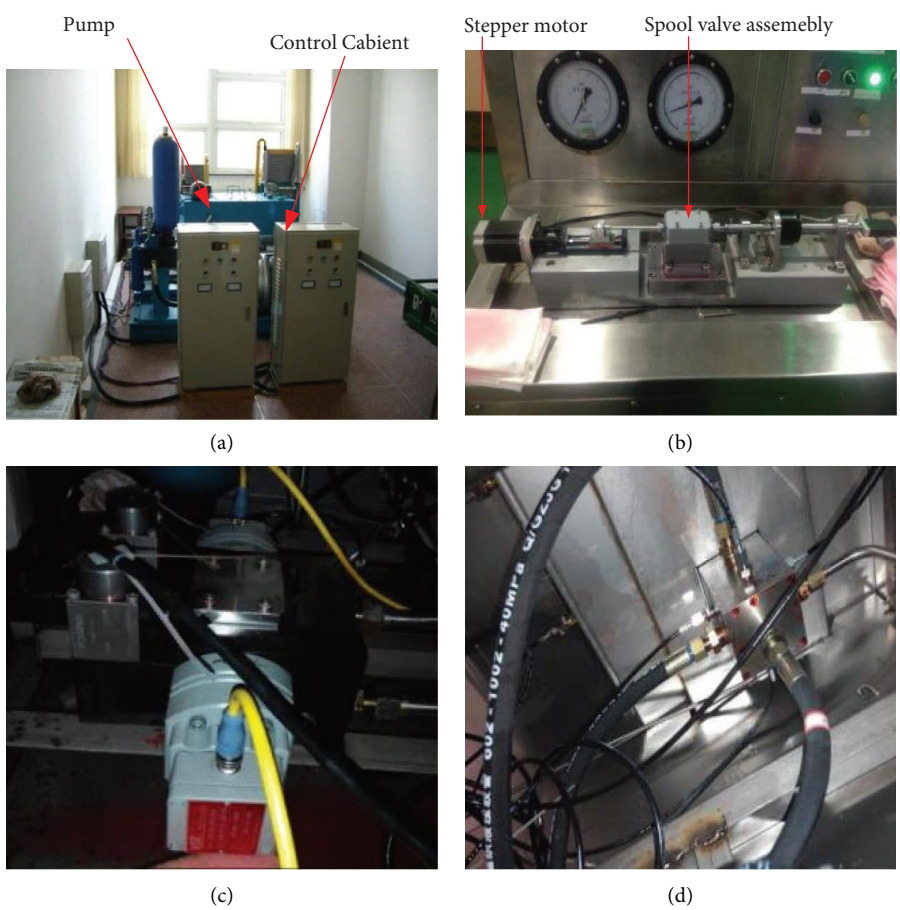

Figure 13: Photo of the experimental setup: (a) oil supply system, (b) spool valve drive system, (c) flowmeter, and (d) oil circuit connection photo at the bottom of the spool valve.

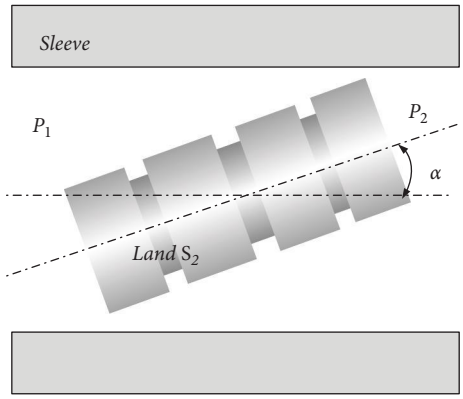

Figure 14: Diagrammatic sketch of boundary conditions for S_2.

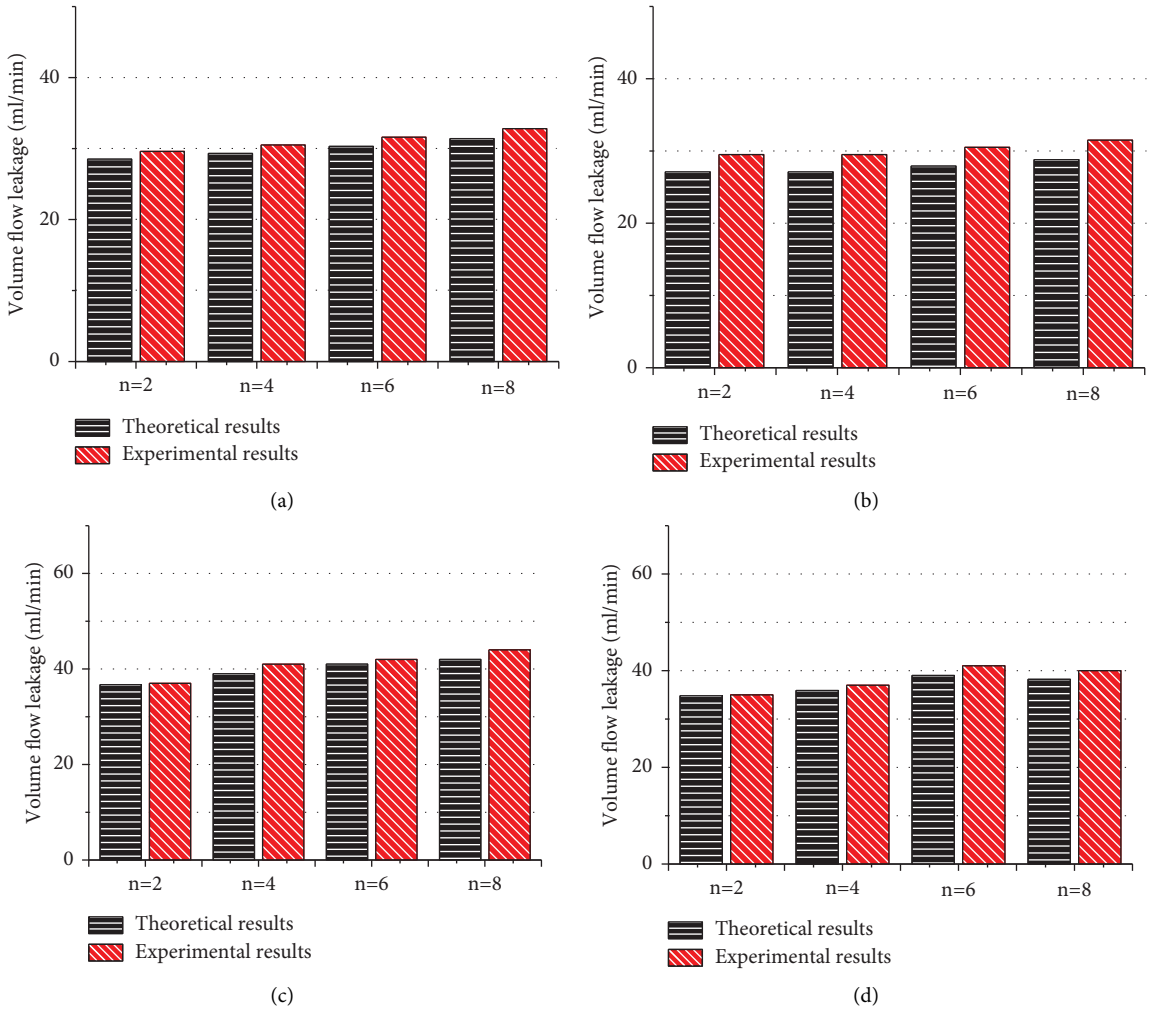

Figure 15: Continued.

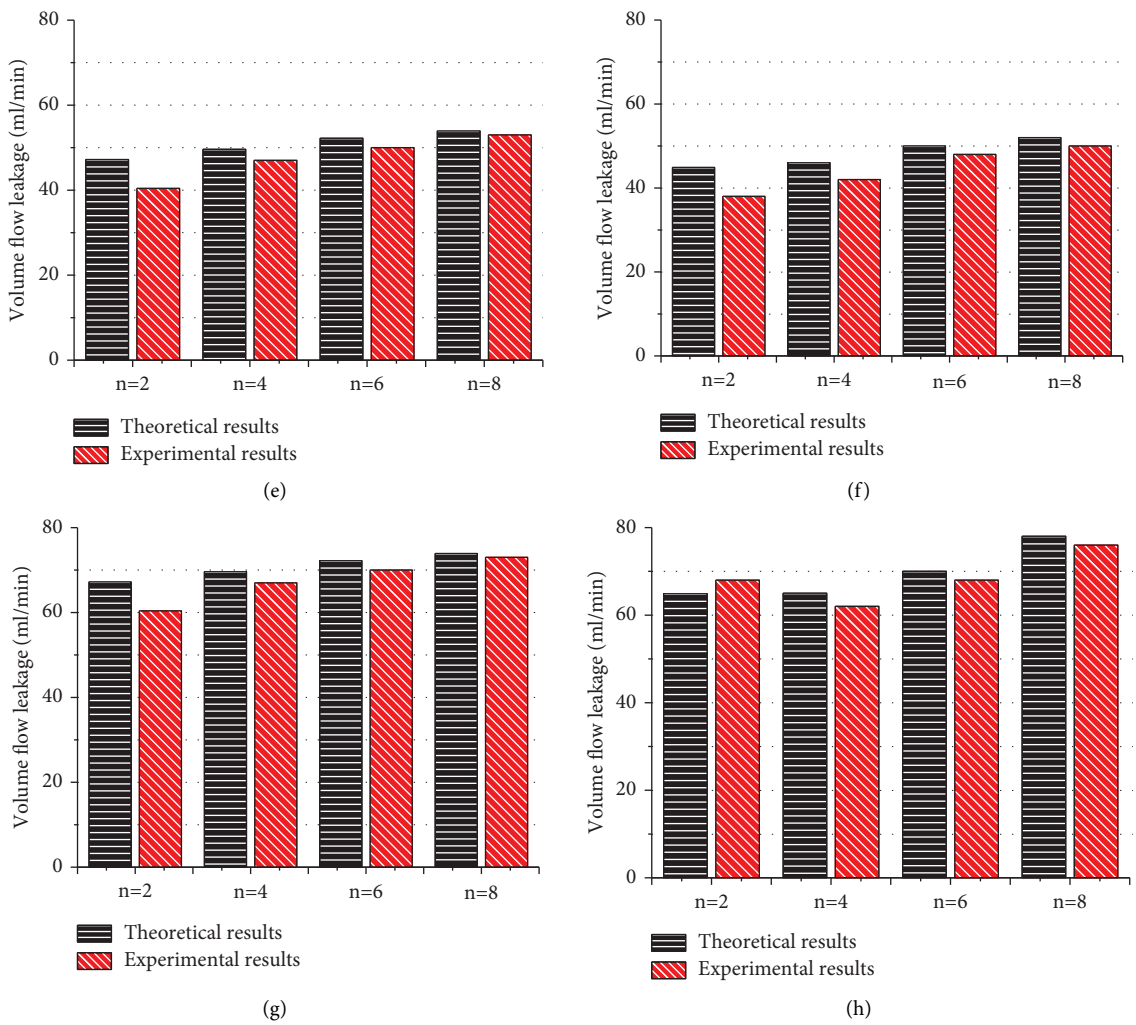

Figure 15: Volume flow leakage comparison between theoretical results and experimental results: (a) $P_d = 5$ MPa, $\alpha = 0.0188^\circ$, (b) $P_d = 5$ MPa, $\alpha = 0.0288^\circ$, (c) $P_d = 7$ MPa, $\alpha = 0.0188^\circ$, (d) $P_d = 7$ MPa, $\alpha = 0.0288^\circ$, (e) $P_d = 9$ MPa, $\alpha = 0.0188^\circ$, (f) $P_d = 9$ MPa, $\alpha = 0.0288^\circ$, (g) $P_d = 35$ MPa, $\alpha = 0.0188^\circ$, and (h) $P_d = 35$ MPa, $\alpha = 0.0288^\circ$.

According to the boundary conditions above, the volume flow leakage rate of the theoretical results and experimental results is compared in Figure 14. The theoretical results and the experimental results both present that the volume flow leakage rate increases with the increase in the number of grooves and the differential pressure. In addition, since under the same inner diameter of the sleeve, the greater the tilted angle of the spool, the smaller the clearance film between the spool and the sleeve, the volume flow leakage rate of the theoretical results decreases with the increase in titled angle, which is just same as that of the experimental results.

Meanwhile, Figure 15 shows that the volume flow leakage of the theoretical results is smaller than that of the experimental results in the cases where the differential pressure is 5 MPa and 7 MPa, but it is the opposite in the case where the differential pressure is 9 MPa and 35 MPa, respectively. With the increase of the differential pressure, the linearity of the theoretical volume flow leakage value is better than that of the experiment, which is more clearly shown in Figure 15. This is because the dynamic viscosity of the fluid increases with the increase in differential pressure, which is ignored in the theoretical model. Nevertheless, the theoretical results are close to the experimental results, which verify the mathematical model derived above.

As shown in Figure 15, the "NS equation" and "Reynolds equation" represent the results obtained by the NS equation and the Reynolds equation from reference [21], respectively. The comparison results show that the volume flow leakage obtained by the NS equation is closer to the experimental results than that obtained by the Reynolds equation. For instance, the maximum percentage of the difference between the results obtained from the Reynolds equation and experimental results is 14.75% in the case where the differential pressure P_d is 5 MPa, the groove number n is 6, and the tilted angle α is 0.0188°. Under the same condition, the percentage of the difference between the results obtained from the NS equation and experimental results is 5.57%. That is to say, the mathematical model of the spool valve clearance film proposed in this paper is more accurate than the models derived from the Reynolds equation.

6. Conclusions

This study establishes an accurate mathematical model of the pressure distribution in the clearance film between the sleeve and the spool with rectangular grooves. This model was derived from the NS equation in cylindrical coordinates and can be used to calculate the uneven pressure distribution, lateral force, and volume flow leakage for the incompressible, isothermal, and Newtonian flow in the clearance film between the sleeve and the spool in different configurations such as geometric dimensions of the spool width, depth, and number. In addition, the values of the volume flow leakage obtained by the mathematical model are compared with that obtained by the experiment under various boundary conditions. The theoretical results and the experimental results indicate conclusions as follows:

(1) Compared with the experimental results, the mathematical model derived from the NS equation could more accurately calculate the lubricant characteristics of the fluid in the clearance film between the sleeve and the spool with rectangular grooves than the model derived from the Reynolds equation in the case of various parameters. However, the effect of the dynamic viscosity changes due to the differential pressure on the uneven pressure distribution required in the future.

(2) The uniformly distributed grooves provide a more effective lubricant characterized along the circumference, mitigating the unbalance pressure distribution. Furthermore, the theoretical results suggested that the wider, deeper, and more number of grooves could more effectively mitigate the unbalanced pressure distribution. In other words, an increase in the cross-sectional area of the groove could effectively decrease the lateral force acting around the spool.

Although the increase in cross-sectional area of the groove could reduce the lateral force, it also degrades the performance of the spool valve. For instance, the increase in volume flow leakage owing to the increment of the number of grooves reduces the driving energy of the spool. Meanwhile, the increment of the depth of the groove reduces the structural strength of the spool. In addition, the mathematical model established in this paper neglects the variation of dynamic viscosity with pressure although the theoretical results are close to the experimental results.

Data Availability

The (groove_with_L2_change_n_8.m) data used to support the findings of this study are included within the article. The (groove_with_L2_change_n_8.m) data present the lateral force in the case where P1 = 7 MPa, $\alpha = 0.288$ degree, K = 1, and $l_2 = 0.2$ mm. The data can be run in MATLAB R2016b.

Conflicts of Interest

The authors declare that they have no conflicts of interest.

Acknowledgments

This work was supported by the National Science Foundation of China (Grant No. U20B2029), National Natural Science Foundation of China (Grant No. 52174005), Natural Science Research Program of the Department of Science and Technology of Shaanxi Provincial (Grant No. 2020JQ-776), (Grant No. 2021KW-33), and (Grant No. 2022JM-305).

References

[1] D. C. Sweeny, "Preliminary investigation of hydraulic lock," *Engineering*, vol. 51, no. 4, pp. 580–582, 1951.

[2] J. F. Blackburn, G. Reethof, and J. L. Shearer, *Fluid Power Control*, pp. 154–196, The Technology Press of MIT and John Wiley, New Jersey, American, 1966.

[3] H. E. Merritt, *Hydraulic Control Systems*, Wiley, New York, NY, USA, 1967.

[4] J. Mannam, "Further aspects of hydraulic lock," *Proceedings - Institution of Mechanical Engineers*, vol. 173, no. 1, pp. 699–716, 1959.

[5] N. Herakovi£, "Flow-force analysis in a hydraulic sliding-spool valve," *Strojarstvo*, vol. 51, no. 6, pp. 555–564, 2009.

[6] T. J. Viersma and B. W. Andersen, "Analysis, synthesis and design of hydraulic servosystems and pipelines," *Journal of Dynamic Systems, Measurement, and Control*, vol. 103, no. 1, pp. 73–86, 1981.

[7] N. Meikandan, R. Raman, M. Singaperumal, K. Seetharamu, and N. Seetharamu, "Theoretical analysis of tapered pistons in high speed hydraulic actuators," *Wear*, vol. 137, no. 2, pp. 299–321, 1990.

[8] M. Borghi, "Hydraulic locking-in spool-type valves: tapered clearances analysis," *Proceedings of the Institution of Mechanical Engineers - Part I: Journal of Systems & Control Engineering*, vol. 215, no. 2, pp. 157–168, 2001.

[9] M. Milani, "Designing hydraulic locking balancing grooves," *Proceedings of the Institution of Mechanical Engineers - Part I: Journal of Systems & Control Engineering*, vol. 215, no. 5, pp. 453–465, 2001.

[10] D. J. Song, D. K. Seo, and W. W. Schultz, "A comparison study between Navier-Stokes equation and Reynolds equation in lubricating flow regime," *KSME International Journal*, vol. 17, no. 4, pp. 599–605, 2003.

[11] C. Guardino, J. W. Chew, and N. J. Hills, "Calculation of surface roughness effects on air-riding seals," *Journal of Engineering for Gas Turbines & Power*, vol. 126, no. 1, pp. 75–82, 2004.

[12] T. Almqvist and R. Larsson, "Some remarks on the validity of Reynolds equation in the modeling of lubricant film flows on the surface roughness scale," *Journal of Tribology*, vol. 126, no. 4, pp. 703–710, 2004.

[13] M. B. Dobrica and M. Fillon, "Reynolds model suitability in simulating Rayleigh step bearing thermohydrodynamic problems," *Tribology Transactions*, vol. 48, no. 4, pp. 522–530, 2005.

[14] M. B. Dobrica and M. Fillon, "About the validity of Reynolds equation and inertia effects in textured sliders of infinite width," *Proceedings of the Institution of Mechanical Engineers - Part J: Journal of Engineering Tribology*, vol. 223, no. 1, pp. 69–78, 2009.

[15] Y. Feldman, Y. Kligerman, I. Etsion, and S. Haber, "The validity of the Reynolds equation in modeling hydrostatic effects in gas lubricated textured parallel surfaces," *Journal of Tribology*, vol. 128, no. 2, pp. 345–350, 2006.

[16] A. Kraker, R. Ostayen, A. V. Beek, and D. Rixen, "A multiscale method modeling surface texture effects," *Journal of Tribology*, vol. 129, no. 2, pp. 485–497, 2007.

[17] J. Li and H. Chen, "Evaluation on applicability of Reynolds equation for squared transverse roughness compared to CFD," *Journal of Tribology*, vol. 129, no. 4, pp. 963–967, 2007.

[18] Q. p. Chen, H. Ji, H. h. Xing, and H. k. Zhao, "Experimental study on thermal deformation and clamping force characteristics of hydraulic spool valve," *Engineering Failure Analysis*, vol. 129, no. 2, pp. 105698–105715, 2021.

[19] L. Schmidt, S. Ketelsen, M. H. Brask, and K. A. Mortensen, "A class of energy efficient self-contained electro-hydraulic drives with self-locking capability," *Energies*, vol. 12, no. 10, pp. 1866–1926, 2019.

[20] S. H. Hong and K. W. Kim, "The validity of the Reynolds equation in spool valve analysis considering cavitation," *Friction*, vol. 4, no. 3, pp. 266–276, 2016.

[21] Q. Lu, J. Tiainen, M. Kiani-Oshtorjani, and Y. Wu, "Lateral force acting on the sliding spool of control valve due to radial flow force and static pressure," *IEEE Access*, vol. 9, Article ID 126658, 2021.

[22] A. Chávez and O. De Santiago, "Determining a pressure response function of the hose and sensor arrangement for measurements of dynamic pressure in a dry gas seal film," *Tribology International*, vol. 143, Article ID 106007, 2020.

[23] J. Jiang, W. Zhao, X. Peng, and J. Li, "A novel design for discrete surface texture on gas face seals based on a superposed groove model," *Tribology International*, vol. 147, Article ID 106269, 2020.

[24] H. Zhao, H. Su, and G. Chen, "Analysis of total leakage of finger seal with side leakage flow," *Tribology International*, vol. 150, Article ID 106371, 2020.

[25] R. Yan, H. Chen, W. Zhang, X. Hong, X. Bao, and X. Ding, "Calculation and verification of flow field in supercritical carbon dioxide dry gas seal based on turbulent adiabatic flow model," *Tribology International*, vol. 165, Article ID 107275, 2022.

[26] X. Wang, L. Shi, Q. Dai, W. Huang, and X. Wang, "Multi-objective optimization on dimple shapes for gas face seals," *Tribology International*, vol. 123, pp. 216–223, 2018.

[27] S. H. Hong and K. W. Kim, "A new type groove for hydraulic spool valve," *Tribology International*, vol. 103, pp. 629–640, 2016.